Basal level of p53 regulates cell population homeostasis

Ann Rancourt[1,2], Sachiko Sato[1], and Masahiko S. Satoh[2]*

[1]Glycobiology and Bioimaging Laboratory of Research Center for Infectious Diseases, and

[2]Laboratory of DNA Damage Responses and Bioimaging, Research Centre of CHUQ,

Faculty of Medicine, Laval University, 2705 Boulevard Laurier, Quebec, Quebec, G1V

4G2, Canada

*Correspondence to: Masahiko S. Satoh

TEL: 1-418-525-4444 ext. 47340

FAX: 1-418-654-2159

e-mail: Masahiko.sato@crchul.ulaval.ca

Abstract

p53 regulates a broad range of processes in cells exposed to various stresses. Although, in unstressed cells, p53 is maintained at low levels, it is unclear if these low levels of p53 have any functional roles. Thus, we investigated the roles of basal levels of p53 using a single-cell lineage tracking technique. We compared the spatiotemporal responses of p53-proficient cancer cells with cells in which p53 gene expression had been silenced. We found that the p53-proficient cell population included a subpopulation of fast-growing cells with a shorter cell-doubling time than other slow-growing cells. p53 silencing reduced the cell-doubling time of the slow-growing cells, thus converting them to faster growing cells. In contrast, the growth rate of the fast-growing cells was unaffected by basal levels of p53, suggesting that growth of slow-growing but not fast-growing cells were regulated by p53 levels. In addition, silencing p53 increased the incidences of multipolar cell division and cell death among the slow-growing cells. These results suggest that basal levels of p53 act to maintain a balance between the fast- and slow-growing cell subpopulations and to suppress the occurrence of abnormal cellular events. We therefore propose that basal levels of p53 help to control cell population homeostasis by regulating the growth and maintaining the integrity of slow-growing cells.

Introduction

The p53 global network regulates various processes, including cell cycle checkpoint control, the DNA damage response pathway, apoptosis, autophagy, and metabolic checkpoint control (*1*). This network governs the ability of p53 to respond flexibly to cellular stresses (*1*). For example, cell cycle progression can be blocked at G1/S or the G2/M boundary following the detection of double-strand DNA breaks through stabilization of p53 in cells exposed to genotoxic stress (*2-8*). If the breaks cannot be repaired, apoptosis is then induced by a p53-mediated mechanism (*9, 10*). These responses are essential for preventing the propagation of cells carrying gene mutations, thereby counteracting the expansion of tumor cells (*1*). Activation of these pathways requires exposure to high doses of genotoxic substances that stabilize p53 (*8, 11-13*), while basal levels of p53 in cells under physiological conditions are maintained low, via an Mdm2-mediated mechanism (*11-13*). However, silencing of p53 in mouse embryonic cells reduced cell cycling time (*14*), suggesting that basal levels of p53 may also have a function, though the roles remain unclear.

We previously developed a novel, chronological, single-cell-lineage tracking system to analyze heterogeneity among cultured cells at the single-cell level by continuous recording of cellular events and movements of live cultured cells using differential contrast imaging (DIC) (*15*). Resulting live cell imaging videos, which contained multidimensional information, including morphology of cells, position of individual cells within a cell population and types of cellular events occurred in a cell. This approach allowed us to extract critical information of individual cells by performing single-cell tracking and creating cell-lineage database. We therefore adopted this system to investigate the role of basal levels of p53 by monitoring and comparing the spatiotemporal responses of p53-proficient A549 lung carcinoma cells and p53 gene-silenced A549 cells. We also examined the responses of cells to non-lethal genotoxic stress. Although high doses of ionizing radiation and radiomimetic agents have been used to induce double-strand DNA breaks and stabilize p53 (*3, 4, 16*), they also generate extensive single-strand DNA breaks and various types of DNA base damage (*17*). We therefore used

the alkylating agent, *N*-methyl-*N*'-nitro-*N*-nitrosoguanidine (MNNG), at a concentration of 1.75 μM (MNNG1.75), which is non-cytotoxic in A549 cells, to study the responses of the cells to non-lethal stress induced by DNA base damage.

Results

Single-cell-lineage tracking analysis of p53 gene-silenced A549 cells

Cells were transfected with scrambled small interfering RNA (siRNA) (Control cells) or p53 siRNA using a lipid-cased transfection method to silence p53 expression (p53(-) cells), and both cell types were exposed to MNNG1.75 (Control+MNNG1.75 and p53(-)+MNNG1.75) (see Movies S1–4). We confirmed that > 99% of cells incorporated siRNA by monitoring the formation of lipid droplets (see Movie S5). We designated the time that tracking started as Time 1, and cells identified at Time 1 were referred to as progenitor cells. We created a cell-lineage database and maps based on the tracking data, and found that the fates of the A549 cells varied (see Figs. S1–4), as shown previously for cervical cancer-derived HeLa cells (*15*).

Reduced cell-doubling time of p53(-) cells

We analyzed the effects of p53 gene silencing on the cell-doubling time of individual A549 cells. The results obtained from the analyses of cell-lineage databases corresponding to videos created by two independent live-cell imagings are shown in Fig. 1A (imaging 1 and 2). The mean cell-doubling times of p53(-) cells in both analyses were consistently shorter than that of Control cells, confirming the reproducibility of the analysis (*18*). We thus created one Control and one p53(-) cell-lineage database by merging the databases created by the two independent imagings, and used these for the following analyses. The mean cell-doubling times for Control and p53(-) cells determined by the merged database were 2204 and 1944 min, respectively (Fig. 1B). We also determined the mean cell-doubling times by curve fitting using a Gaussian distribution, and the times for Control and p53(-) cells were 1,819 min and 1,588 min, respectively (Fig. 1C and D), suggesting that p53 silencing was associated with a reduction in cell-doubling time. This was confirmed by statistical analysis based on the distribution of cell-doubling times of individual cells (Fig. 1B), indicating that loss of basal p53 expression shortened the cell-doubling time. In contrast, there was no significant difference in cell-doubling time between

MNNG-treated Control and MNNG-treated p53(-) cells, while the doubling times of these treated cells were significantly longer than those of untreated Control and p53(-) cells (Fig. 1B), suggesting that low-level alkylated base damage prolonged cell-doubling times of A549 cells, regardless of the presence or absence of basal levels of p53.

Cell-doubling time of p53(-) progenitor cells and their progeny

We assessed the duration of the p53-silencing effect by determining the cell-doubling times of the progenitor cells, and their daughter and granddaughter (GD) cells. As defined above, progenitor cells were cells identified at Time 1, and were thus produced prior to or during siRNA treatment. We thus determined cell-doubling times by analyzing videos taken during siRNA treatment. The cell-doubling time of p53(-) progenitor cells was significantly shorter than that of Control cells (Fig. 2A). Furthermore, the cell-doubling times of p53(-) daughter and GD cells were also significantly shorter than their control counterparts (Fig. 2B). The cell-doubling times of both Control and p53(-) GD cells were significantly longer than those of their respective daughter cells, possibly due to the increased cell density. Nonetheless, the effect of p53 silencing was maintained through at least two cell divisions and silencing p53 consistently shortened the cell-doubling times. Cell growth curves determined after *in silico* cell cycle synchronization (Fig. 2C) showed a significant increase in p53(-) cells (Fig. 2D and E), confirming that the reduced cell-doubling time of p53(-) cells resulted in their increased growth.

Analysis of multipolar cell division, cell death, and cell fusion

To gain further insights into the events induced by p53 silencing, we investigated if p53 silencing induced tripolar cell division, cell death, or cell fusion in A549 cells, given that tripolar cell division (*19, 20*), cell death, and cell fusion were previously reported to occur during the proliferation of HeLa cells (*15*). We determined the number of bipolar cell divisions as a reference, and showed that there were significantly more bipolar divisions in p53(-) compared with Control cells (Fig. 3A), consistent

with increased cell growth (Fig. 2D and E). Multipolar spindle formation has been reported to occur frequently in p53-deficient cancer cells, and tripolar cell division has also often been reported in malignant cancer cells (*21-24*). Interestingly, the frequency of tripolar cell divisions was significantly increased by p53 silencing (Fig. 3B), while cell death was also significantly increased (Fig. 3C). Furthermore, cell death in p53(-) cells (Movie S6) was distinct from that induced in Control cells by exposure to high-dose MNNG (40 μM; Movie S7). Finally, p53 silencing also increased cell fusion, which could affect cell ploidy (Fig. 3D). These results suggest that, in addition to regulating the cell-doubling time, basal levels of p53 also have a function in suppressing abnormal cellular events.

Analysis of cell subpopulations

Our results suggest that p53 silencing resulted in a reduction of cell-doubling time, and increases in tripolar cell division, cell death, and cell fusion. As noted above, A549 cells comprise cells with different growth abilities (Figs. S1–4), and it is not clear if the above reduction and increase occurred in a specific subgroup of A549 cells. We therefore grouped progenitor cells on the basis of the numbers of progeny present at 5,980 min (Group A, 0–1; B, 2–3; C, 4–5; D, 6–7; and E, ≥ 8 cells) (Table 1). As shown in Fig. 4 A and B, the most rapidly-growing cells belonged to Group E, which increased from 10.75 (total number of cells at Time 1 normalized by 100) to 92.75 cells (8.3-fold increase) during 5,980 min of cell culture (Fig. 4A; Table 1); p53(-) Group E cells were more abundant than Control cells at Time 1 (19.95 cells) (Fig. 4B; Table 1), suggesting that less-fast growing cells (Groups A–D cells) were converted into fast-growing cells by p53 silencing. These Group E cells were thus composed of cells that already had a fast-growing ability and cells in which the growing ability was promoted by p53 silencing. To evaluate the cell-doubling time of each group, we analyzed the cell-doubling times of Group B–E daughter cells. Among Control cells, cells in Group B showed the longest mean cell-doubling time, and the doubling time was reduced in line with the increase in growth ability, with Group E cells showing the shortest mean cell-doubling time (Fig. 4C). While p53 silencing

significantly reduced the mean cell-doubling time of cells in Group B and C (Fig. 4C), the mean cell-doubling time of the fast-growing cells (Group E) was unaffected by p53 silencing. These results suggest that fast-growing cells retained their short cell-doubling time and high proliferation ability, regardless of the presence or absence of p53 whereas the growth of the remaining, slower-growing cell populations was regulated by basal levels of p53. Furthermore, tripolar cell division (Fig. 4D), cell death (Fig. 4E), and cell fusion (Fig. 4F) were all more frequent in p53(-) cells from Groups A and B, suggesting that basal levels of p53 also have a function in maintaining the integrity of slow-growing cells.

Cell division times of daughter cells

To gain further evidence to support a role for basal levels of p53 in the growth of slow-growing but not fast-growing cells, we compared differences in cell-doubling times among daughter cells. If basal p53 levels affected the cell-doubling time of slow-growing cells, we anticipated that the cell-doubling times of individual cells would vary, as the levels of regulation would differ. We would therefore expect slow-growing Control daughter cells to show larger differences in cell-doubling times than p53(-) cells and Group E Control cells (Fig. 5A). Indeed, differences in cell-doubling times were significantly larger among Group C Control cells compared with p53(-) cells (Fig. 5B Group C, Control vs p53(-)), indicating that basal p53 levels played a role in controlling cell-doubling time in this group. The mean difference in cell-doubling time in Group D control cells was lower than that in Group C cells, and this was further reduced in Group E cells. Furthermore, there was no significant difference between in cell-doubling time differences between Group E Control and p53(-) cells. These results suggest that basal p53 levels had no major impact on the growth of Group E cells, distinct from Group C cells, and consistent with the results shown in Fig. 4C.

Responses of p53(-) cells to exposure to MNNG1.75

MNNG1.75 significantly increased the cell-doubling time of both Control and p53(-) cells (Fig. 1D). We therefore explored the effect of exposure of cells to non-cytotoxic low-dose MNNG1.75, and showed that this dose reduced the numbers of progeny of both Control and p53(-) cells in Groups D and E (Table 1). Importantly, this dose of MNNG1.75 did not increase cell death (Fig. 3C), indicating that the reductions in Group D and E cells were due to suppression of cell growth, rather than increased cell death (Table 1). Furthermore, MNNG1.75 significantly increased the differences in cell-doubling times of both Control and p53(-) cells (Fig. 5B), suggesting that basal levels of p53 were not involved in the response to non-cytotoxic levels of base damage.

Discussion

In the present study, we demonstrated that the growth and integrity of A549 lung carcinoma cells were controlled by basal levels of p53 (Fig. 5C). Normal (p53-proficient) cells are composed of subpopulations of cells with different doubling times. The growth of most of these cells (slow-growing cells) is controlled by basal levels of p53 through regulation of their cell-doubling time, while the cell-doubling time of the other, fast-growing cells is unaffected by basal p53. Removal of basal levels of p53 reduces the cell-doubling time of the slow-growing subpopulation, thus increasing the proportion of fast-growing cells. We previously reported that HeLa cells contained a fast-growing cell population (about 3%–7%) (*15*). If all the progeny of fast-growing cells retained a high proliferative ability, the overall growth rate of cells would be expected to increase at every cell passage; however, no such increase occurs. We therefore previously proposed that some progeny of fast-growing cells are converted into slow-growing cells, thus maintaining a constant fast-growing cell population. This pattern of cell growth whereby cells produce both fast-growing progeny to replace themselves, as well as slow-growing progeny, resembles the situation in stem cells, and we therefore referred to these cells as putative cancer stem cells (*15*). The presence of fast- and slow-growing cells allows the cell population to maintain its homeostasis by balancing the rate of self-renewal of stem cells and the production of "differentiated" cells. Although A549 cells are cancer cells, it is possible that they may retain characteristics of their ancestral normal lung tissue cells, such that if fast-growing A549 cells are defined as putative cancer stem cells, slow-growing A549 cells may correspond to some type of differentiating cells. We thus propose that basal levels of p53 may play a role in controlling cell population homeostasis by regulating the growth of the slow-growing cells.

We also found that removal of basal p53 levels increased tripolar cell division, cell death, and cell fusion among slow-growing cells (Fig. 5C, p53 deficient cells). The p53 gene is known to be mutated in > 50% of malignant human cancers, which also frequently show tripolar cell division (*22-26*). Our results were therefore consistent with earlier observations, and imply that basal levels of p53 may also

help to maintain the integrity of slow-growing cells and p53 gene mutations occurred in slow-growing cells may result in the formation of malignant cells. It is also plausible that p53 gene mutations occur in fast-growing cells and the effect of the mutations became evident upon "differentiation" of fast-growing cells into slow-growing cells. Nevertheless, it may be critical to understand the process, through which DNA damage formation leads to p53 gene mutations in the slow- and/or fast-growing cells to further reveal a link between the loss of p53 function and malignant tumor formation.

Our results also suggest that basal levels of p53 are not involved in the cellular response to non-lethal levels of alkylated base damage, as the formation of the levels of base damage suppressed growth of both Control and p53(-) cells (Fig. 5D). High doses of genotoxic substances, e.g. ionizing radiation and radiomimetic agents (*3, 4, 16*), have frequently been used in the study of p53; however, these substances produce large amounts of base damage and single-strand DNA breaks, in addition to more minor double-strand DNA breaks, which activate p53-dependent DNA-damage responses (*8, 16, 27, 28*). These base damage and single-strand DNA breaks do not necessarily directly activate p53-mediated responses, thus, while p53-mediated responses are induced by the formation of double-strand DNA breaks, cellular function may be severely influenced by other forms of damage, given that even non-lethal levels of alkylated base damage significantly suppress growth of Control and p53(-) cells. However, it would be interesting to consider if the lack of p53-mediated responses to base damage, including the pre-mutagenic DNA lesions, O^6-alkylguanine and 8-hydroxyguanine (*29-31*), allow the induction of p53 gene mutations, such that p53-mutated malignant tumor cells may be produced as a result of exposure to alkylating agents or reactive oxygen species.

Materials and Methods

A549-luc-C8 cells were purchased from Xenogen Corporation and cultured in RPMI containing 10% fetal bovine serum in a humidified 5% CO_2. To plate cells onto a coverglass Lab-Tek 8 well chamber, 50 µl of A549 cell suspension containing 3500 cells were placed at the center of each well and left until cells attached to the coverglass surface. Then, 0.75 ml of culture medium was added to each well. The Lab-Tek 8 well chamber was placed on a microscope stage after 24 h of plating and lipofection of p53 siRNA or scrambled control RNA (New England Bio Labs) was performed. After 24 h of treatment, cells were exposed to MNNG1.75 (Sigma-Aldrich) for 30 min in serum-free RPMI, and the medium was replaced with fresh RPMI containing 10% fetal bovine serum.

Long-term live cell imaging and data analysis

Quorum WaveFX Spinning Disc Confocal System (Quorum Technologies Inc., Canada) with Leica microscope controlled by Volocity v4.0 was used for long-term live cell imaging. DIC images were taken through HCX PL APO 40x oil objectives (NA=1.25) by using a Halogen lamp as a light source. Cells that were grown on a coverglass Lab-Tek 8 well chamber were then placed on a microscope stage and were cultured using an environmental chamber at 37ºC with 7.5% humidified CO_2 (Pathology Devices Inc, MD). In each well, a two-dimensional image acquisition array (fields of view: FOVs) was made to cover the area of interest (*15*). XY positions of FOVs were then registered using Volocity v4.0. DIC images were captured every 10 min from + 10 to – 10 µm of the focal plane at every 1 µm using piezo focus drive. Exposure time was normally 34 msec. To make time-lapse movies, focused images were selected from 21 *z*-plane image files. Volocity image sequence files were used to select the optimal focal plane for each FOV. Then, the image sequence files were split into independent files to select focal plane files. After the selection, files containing focused image were assembled into a movie using QuickTime Player Pro. Live cell imaging started at the beginning of siRNA treatment, and continued during the treatment of cells with serum-free medium or the medium with MNNG1.75. Then, after the replacement

of the medium to RPMI containing 10% fetal bovine serum, imaging was continued for 5,980 minutes (99.7 hours). Cell tracking was started at the end of the treatment with serum-free medium or the medium with MNNG1.75, and the time that started the tracking is designated as Time 1. Panorama views of Time 1 were prepared and cell lineage numbers were assigned to cells in a selected area (*15*). After assigning the cell lineage numbers, each cell was tracked using QuickTime Player Pro and the time points that mitosis, bipolar cell division, tripolar cell division, cell death and cell fusion occurred in each cell were determined. To draw cell lineage maps and process data, C/C++ programs were written. About 200 each of progenitor cells were selected from imaging videos that were created by independent long-term live cell imaging, and total 200-400 progenitor cells and its progeny were tracked. In the single-cell lineage tracking analysis, a multi-well chamber was used to simultaneously obtain images of Control and p53(-) cells, as well as cells exposed MNNG1.75, so that alterations occurring in the cells can be accurately analyzed.

Determination of cell-doubling times

We used a cell-lineage database to determine cell-doubling times of individual cells. The time when a cell was produced by cell division (Time A) and the time when the same cell produced daughter cells (Time B) were determined, and cell-doubling time was calculated by subtracting Time A from Time B. In the case of progenitor cells (Fig. 2A), these cells were produced prior to or during siRNA treatment. Thus, we determined Time A by analyzing videos taken during siRNA treatment.

Statistical analyses of cell-doubling times

Cell-doubling times were analyzed by Student's *t*-tests (unpaired and two-tailed) or one way ANOVA using Prism 7.

Statistical analyses of cell growth

The number of progenitor cells and/or progeny of each cell lineage found at 5980 min was determined. The data were analyzed by one way ANOVA using Prism 7.

Statistical analyses of cellular events

The number of bipolar cell division, tripolar cell division, cell death, and cell fusion occurred in each cell lineage found at 5980 min was determined. The data were analyzed by or one way ANOVA using Prism 7.

Acknowledgements

We like to acknowledge Ms. Julie-Christine Lévesque, and the Bioimaging Platform of Research Centre for Infectious Diseases for the technical support of microscopes. This work was supported by the Canadian Foundation for Innovation.

Author contributions

M.S.S. and S.S. designed this work, performed the experiments and wrote the paper. A.R. performed the experiments and single-cell tracking analysis.

References

1. E. R. Kastenhuber, S. W. Lowe, Putting p53 in Context. *Cell* **170**, 1062-1078 (2017).
2. E. Appella, C. W. Anderson, Post-translational modifications and activation of p53 by genotoxic stresses. *Eur J Biochem* **268**, 2764-2772 (2001).
3. J. Brugarolas *et al*., Radiation-induced cell cycle arrest compromised by p21 deficiency. *Nature* **377**, 552-557 (1995).
4. C. Deng, P. Zhang, J. W. Harper, S. J. Elledge, P. Leder, Mice lacking p21CIP1/WAF1 undergo normal development, but are defective in G1 checkpoint control. *Cell* **82**, 675-684 (1995).
5. L. E. Giono, J. J. Manfredi, The p53 tumor suppressor participates in multiple cell cycle checkpoints. *J Cell Physiol* **209**, 13-20 (2006).
6. H. Hermeking *et al*., 14-3-3sigma is a p53-regulated inhibitor of G2/M progression. *Mol Cell* **1**, 3-11 (1997).
7. M. B. Kastan, O. Onyekwere, D. Sidransky, B. Vogelstein, R. W. Craig, Participation of p53 protein in the cellular response to DNA damage. *Cancer Res* **51**, 6304-6311 (1991).
8. S. Y. Shieh, M. Ikeda, Y. Taya, C. Prives, DNA damage-induced phosphorylation of p53 alleviates inhibition by MDM2. *Cell* **91**, 325-334 (1997).
9. A. R. Clarke *et al*., Thymocyte apoptosis induced by p53-dependent and independent pathways. *Nature* **362**, 849-852 (1993).
10. S. W. Lowe, E. M. Schmitt, S. W. Smith, B. A. Osborne, T. Jacks, p53 is required for radiation-induced apoptosis in mouse thymocytes. *Nature* **362**, 847-849 (1993).
11. Y. Haupt, R. Maya, A. Kazaz, M. Oren, Mdm2 promotes the rapid degradation of p53. *Nature* **387**, 296-299 (1997).
12. R. Honda, H. Tanaka, H. Yasuda, Oncoprotein MDM2 is a ubiquitin ligase E3 for tumor suppressor p53. *FEBS Lett* **420**, 25-27 (1997).

13. M. H. Kubbutat, S. N. Jones, K. H. Vousden, Regulation of p53 stability by Mdm2. *Nature* **387**, 299-303 (1997).

14. S. Guo *et al*., Nonstochastic reprogramming from a privileged somatic cell state. *Cell* **156**, 649-662 (2014).

15. S. Sato, A. Rancourt, Y. Sato, M. S. Satoh, Single-cell lineage tracking analysis reveals that an established cell line comprises putative cancer stem cells and their heterogeneous progeny. *Sci Rep* **6**, 23328 (2016).

16. H. W. Yang, M. Chung, T. Kudo, T. Meyer, Competing memories of mitogen and p53 signalling control cell-cycle entry. *Nature* **549**, 404-408 (2017).

17. M. S. Satoh, G. G. Poirier, T. Lindahl, NAD(+)-dependent repair of damaged DNA by human cell extracts. *J Biol Chem* **268**, 5480-5487 (1993).

18. S. Sato. A. Rancourt, M. S. Satoh, Dose-dependent spatiotemporal responses of mammalian cells to an alkylating agent. *BioRxiv* **doi:** https://doi.org/10.1101/215764.

19. N. J. Ganem, S. A. Godinho, D. Pellman, A mechanism linking extra centrosomes to chromosomal instability. *Nature* **460**, 278-282 (2009).

20. Q. Shi, R. W. King, Chromosome nondisjunction yields tetraploid rather than aneuploid cells in human cell lines. *Nature* **437**, 1038-1042 (2005).

21. C. M. Eischen, Genome Stability Requires p53. *Cold Spring Harb Perspect Med* **6**, (2016).

22. J. S. Lanni, T. Jacks, Characterization of the p53-dependent postmitotic checkpoint following spindle disruption. *Mol Cell Biol* **18**, 1055-1064 (1998).

23. J. M. Schvartzman, P. H. Duijf, R. Sotillo, C. Coker, R. Benezra, Mad2 is a critical mediator of the chromosome instability observed upon Rb and p53 pathway inhibition. *Cancer Cell* **19**, 701-714 (2011).

24. I. Vitale *et al*., Multipolar mitosis of tetraploid cells: inhibition by p53 and dependency on Mos. *EMBO J* **29**, 1272-1284 (2010).

25. M. S. Greenblatt, W. P. Bennett, M. Hollstein, C. C. Harris, Mutations in the p53 tumor suppressor gene: clues to cancer etiology and molecular pathogenesis. *Cancer Res* **54**, 4855-4878 (1994).

26. M. Hollstein, D. Sidransky, B. Vogelstein, C. C. Harris, p53 mutations in human cancers. *Science* **253**, 49-53 (1991).

27. C. von Sonntag, *The Chemical Basis of Radiation Biology*. (Taylor & Francis, London, 1987).

28. J. F. Ward, DNA damage produced by ionizing radiation in mammalian cells: identities, mechanisms of formation, and reparability. *Prog Nucleic Acid Res Mol Biol* **35**, 95-125 (1988).

29. J. S. Eadie, M. Conrad, D. Toorchen, M. D. Topal, Mechanism of mutagenesis by O6-methylguanine. *Nature* **308**, 201-203 (1984).

30. B. Myrnes, K. E. Giercksky, H. Krokan, Repair of O6-methyl-guanine residues in DNA takes place by a similar mechanism in extracts from HeLa cells, human liver, and rat liver. *J Cell Biochem* **20**, 381-392 (1982).

31. K. C. Cheng, D. S. Cahill, H. Kasai, S. Nishimura, L. A. Loeb, 8-Hydroxyguanine, an abundant form of oxidative DNA damage, causes G----T and A----C substitutions. *J Biol Chem* **267**, 166-172 (1992).

Figure legends

Fig. 1 Analysis of cell-doubling time.

A. Two sets of videos (Control and p53(-)) created by independent long-term live cell imaging (1 to 5980 min) were used for cell-tracking analysis (Imaging 1 and 2). Cell-doubling times of each cell were analyzed by Student's *t*-tests; $^{****}p<0.0001$. Results shown as mean ± standard error (SEM). **B.** One Control and one p53(-) cell-lineage database were created by merging two cell-lineage databases used for the analysis in frame **A**. Cell-doubling times of Control, p53(-), Control+MNNG1.75, and p53(-)+MNNG1.75 cells were analyzed by one way ANOVA; ns, not significant and $^{****}p < 0.0001$. Results shown as mean ± standard error (SEM). **C and D.** Distributions of cell-doubling times for Control (**C**) and p53(-) cells (**D**) were determined. Mean cell-doubling times and standard deviations were calculated according to a Gaussian distribution (Prism 7).

Fig. 2 Cell-doubling times of progenitor cells, and their daughter and GD cells.

A. The cell-doubling times of the progenitor cells were determined. As defined, progenitor cells were cells identified at Time 1, and were thus produced prior to or during siRNA treatment. We therefore determined cell-doubling times of progenitor cells by analyzing videos taken during siRNA treatment. As siRNA treatment showed an effect on the rate of cell growth, cell-doubling times of the progenitor cells were prolonged compared with that of daughter and DG cells. Student's *t*-tests were performed; $^{****}p<0.0001$. Results shown as mean ± SEM. **B.** Daughter and GD cells were analyzed based on the cell-lineage database and cell-doubling time distributions are shown. One way ANOVA was performed; $^{****}p <0.0001$. Results shown as mean ± SEM. **C.** The cell cycle was synchronized *in silico* and the time point at which the progenitor cells divided was normalized at Time 1 (blue arrowhead). Daughter and GD cells are indicated by green and orange arrowheads, respectively. **D.** Cell growth curves determined after synchronization. **E.** The numbers of cells produced from each progenitor cell at 5,980 min were

calculated and compared by One way ANOVA; $^{**}p < 0.01$, $^{***}p < 0.001$ and $^{****}p < 0.0001$. Results shown as mean ± SEM.

Fig. 3 Analysis of bipolar and tripolar cell divisions, cell death, and cell fusion.

Numbers of bipolar divisions (**A**), tripolar cell divisions (**B**), cell death events (**C**), and cell fusion events (**d**) were determined using the cell-lineage database. One way ANOVA was performed; ns, not significant, $^{*}p < 0.05$; $^{**}p < 0.01$ and $^{****}p < 0.0001$. Results shown as mean ± SEM.

Fig. 4 Analysis of cells in Groups A–E.

A and B. Progenitor cells and their lineages were grouped according to the number of progeny cells (Group A, 0–1; B, 2–3; C, 4–5; D, 6–7; and E, ≥ 8) at 5,980 min. The numbers of Control (**A**) and p53(-) cells (**B**) in each group at each time point were determined. The initial number of cells was normalized by 100. The total numbers of cells at Time 1 and at 5980 min are shown. Small frames show growth curves for each group of cells. **C.** Cell-doubling time distributions for daughter cells of Groups B–E are shown. One way ANOVA was performed; ns, not significant, $^{***}p < 0.001$ and $^{****}p < 0.0001$. Results shown as mean ± SEM. **d–f.** Numbers of tripolar cell divisions (**D**), cell death events (**E**), and cell fusion events (**F**) in each group are shown. Student's *t*-tests were performed in relation to Control; $^{*}p < 0.05$, $^{***}p < 0.001$ and $^{****}p < 0.0001$.

Fig. 5 Differences in cell division times of daughter cells, and role of basal levels of p53 in regulation of cell growth and integrity

A. The differences in cell division times between daughter cells were determined for each cell-lineage. **B.** The distribution of time differences for Groups B–E cells are shown. Group B Control daughter cells did not undergo cell division and the value was therefore infinity. One way ANOVA was performed; ns, not significant; ****$p < 0.0001$. Results shown as mean ± SEM. **C.** p53-proficient cells are

composed of subpopulations with different cell-doubling times. Basal p53 regulates the cell-doubling time of the slow-growing cells (red, yellow and green circles), while the cell-doubling time of the fast-growing cells (light blue and blue circles) is unaffected by basal p53. Removal of basal p53 reduces the cell-doubling time of the slow-growing cells, thereby converting them into faster-growing cells (red arrows) and increasing the overall proportion of fast-growing cells. Removal of basal p53 also increases the incidences of cell death, tripolar cell division, and cell fusion. **D.** Non-lethal levels of base damage in p53-proficient and p53-deficient cells result in prolonged cell-doubling time and suppression of cell-growth. The cells thus respond to base damage in a p53-independent manner.

Table 1. The number of progeny produced from progenitor cells.

Progeny (No.)[1)]	Control		p53(-)		Control+MNNG1.75		p53(-) +MNNG1.75	
	No. of cells (1 min) [2)]	**No. of cells (5980 min) [3)]**	No. of cells (1 min) [2)]	**No. of cells (5980 min) [3)]**	No. of cells (1 min) [2)]	**No. of cells (5980 min) [3)]**	No. of cells (1 min) [2)]	**No. of cells (5980 min) [3)]**
A: 0–1	25.50	**23.25**	20.20	**15.71**	28.62	**26.13**	25.00	**21.00**
B: 2–3	29.50	**65.25**	28.43	**67.33**	43.20	**103.01**	37.00	**89.50**
C: 4–5	22.50	**96.75**	20.20	**87.78**	26.63	**111.06**	31.00	**128.50**
D: 6–7	11.75	**76.75**	11.22	**74.06**	1.05	**6.03**	6.00	**39.00**
E: ≥ 8	10.75	**92.75**	19.95	**179.80**	0.50	**4.02**	1.00	**8.50**
Total	100	**354.75**	100	**424.68**	100	**250.25**	100	**286.5**

[1)] Progenitor cells were grouped on the basis of the numbers of progeny present at 5,980 min (Group A, 0–1; B, 2–3; C, 4–5; D, 6–7; and E, ≥ 8 cells).

[2)] The numbers of progenitor cells present at 1 min are shown. The initial number of cells was normalized by 100.

[3)] The numbers of cells at 5980 min are shown.

Fig. 1

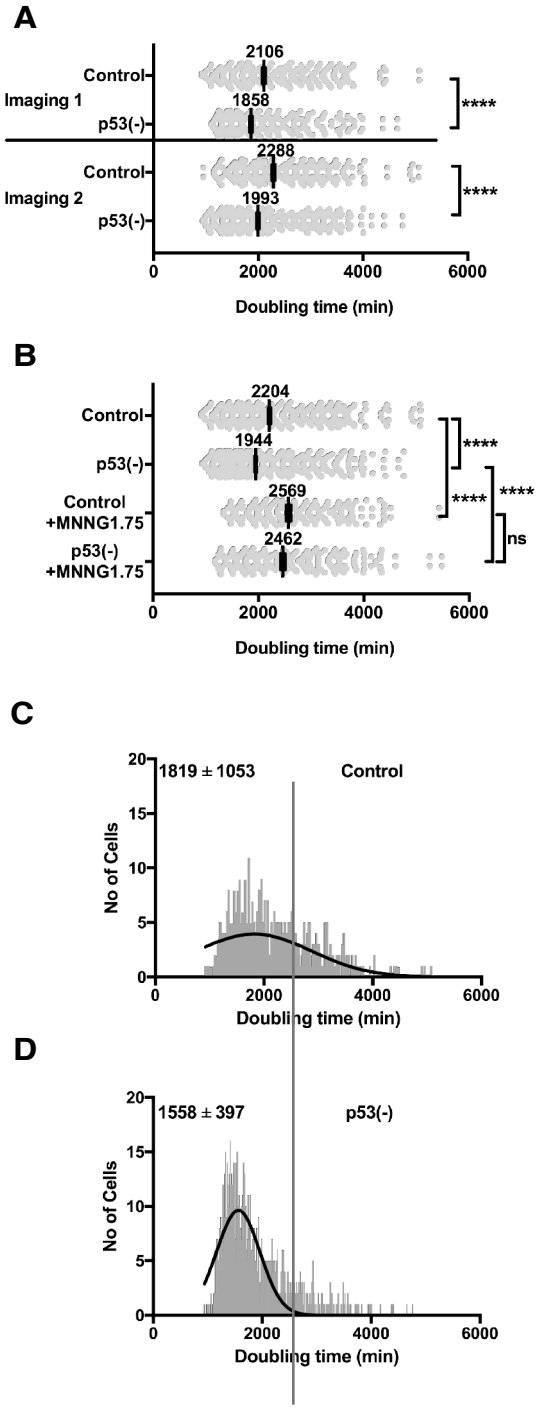

Fig. 2

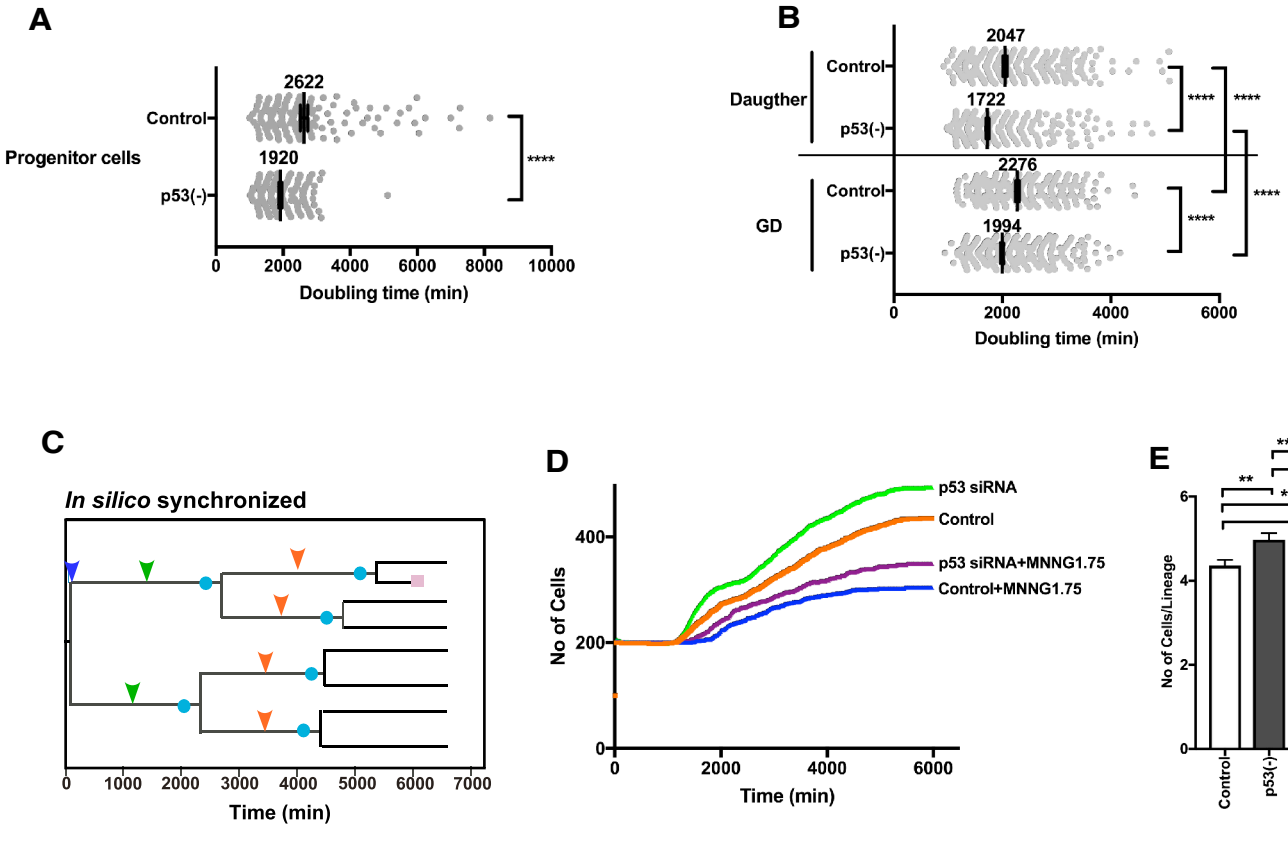

Fig. 3

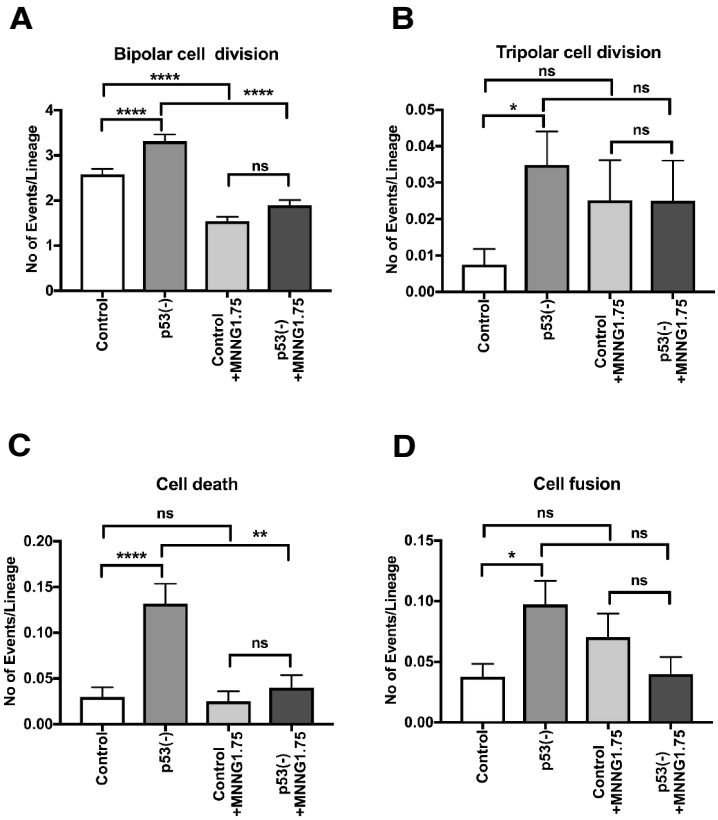

Fig. 4

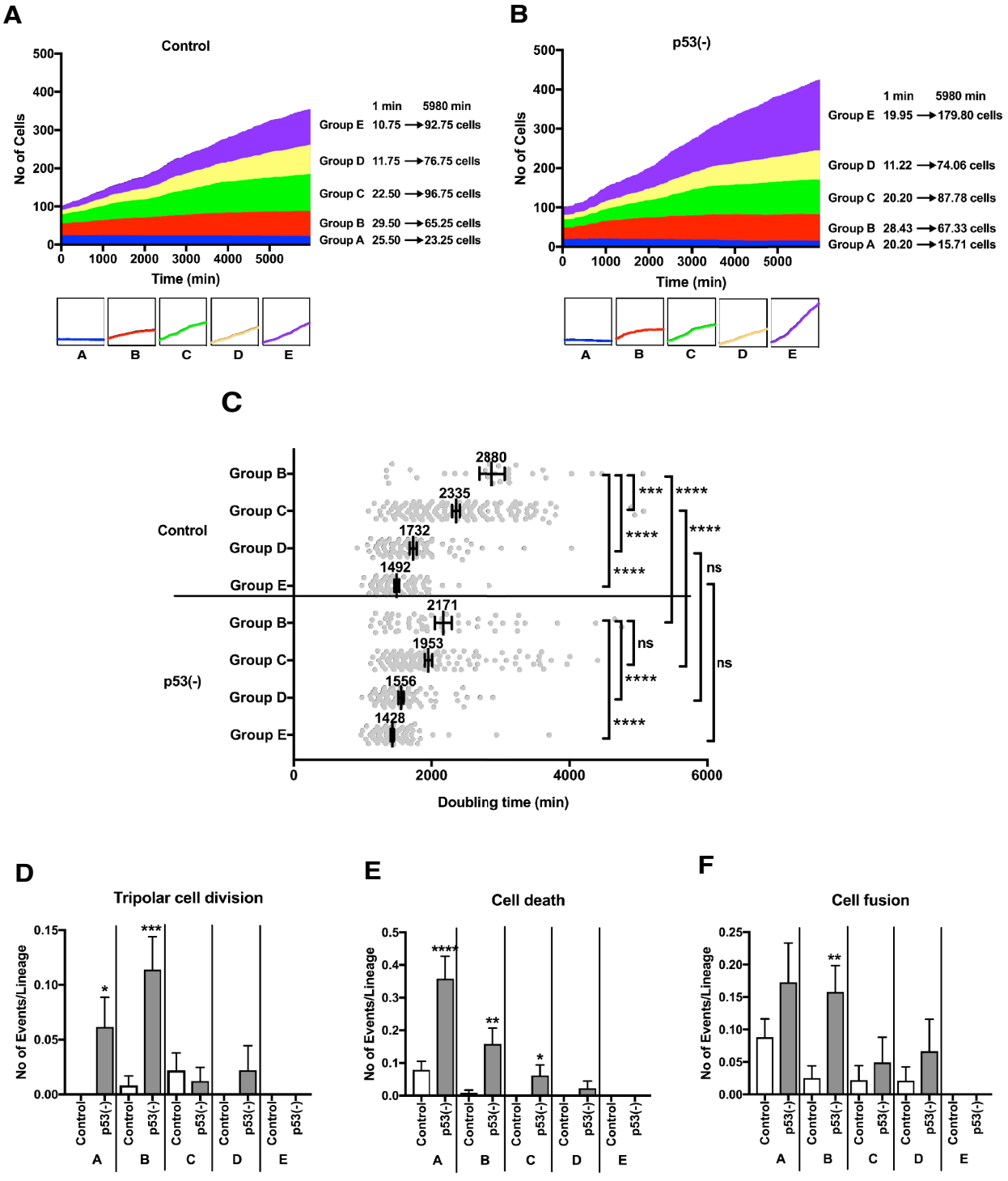

Rancourt et al.

Fig. 5